


Article

# Sedimentary Environmental Evolution of the Western Taiwan Shoal Area since the Late Pleistocene

Chipeng He <sup>1</sup>, Longbin Sha <sup>1,2</sup> , Dongbo Zhao <sup>3</sup>, Lu Dai <sup>1,2</sup>, Zheng Li <sup>1</sup>, Jiabing Tang <sup>1</sup>, Xianfu Li <sup>1</sup>  
and Dongling Li <sup>1,2,\*</sup>

<sup>1</sup> Department of Geography and Spatial Information Technology, Ningbo University, Ningbo 315211, China; 1911073004@nbu.edu.cn (C.H.); shalongbin@nbu.edu.cn (L.S.); dailu@nbu.edu.cn (L.D.); 1911073009@nbu.edu.cn (Z.L.); 51213904003@stu.ecnu.edu.cn (J.T.); xianfuli21@hotmail.com (X.L.)

<sup>2</sup> Institute of East China Sea, Ningbo University, Ningbo 315211, China

<sup>3</sup> Fujian Provincial Key Laboratory of Coast and Island Management Technology Study, Fujian Institute of Oceanography, Xiamen 361013, China; zdb@fjio.net

\* Correspondence: lidongling@nbu.edu.cn; Tel.: +86-574-8760-5546; Fax: +86-574-8760-5546

**Abstract:** A new pollen analysis and major and trace element contents were conducted on a 40 m long gravity core recovered from the Taiwan Shoal (sand ridges), south of the Taiwan Strait, beginning in the Late Pleistocene. The changes in the pollen assemblage and concentration represent the climate change around the Taiwan Shoal and the strength of the Zhe-Min Coastal Current, whereas variations in major and trace element contents can imply the source of the sediments in the Taiwan Shoal, which are correlated with the rise or fall of the sea level with increased marine dinoflagellate cysts. The interval of 40–30 m was characterized by high pollen and spore concentrations, and evergreen *Quercus* was dominant taxon, which indicates a warm sedimentary environment, and the surrounding area of the Taiwan Shoal were covered by a tropical and subtropical broad-leaved forest. There were no pollen and spores from 30–24 m, which indicates a strong hydrodynamic sedimentary environment, and most of the Taiwan Shoal might have been experience subaerial exposure. The interval of 24–17 m was characterized by the reappearance of pollen and spores, as well as marine dinoflagellate cysts and foraminifera, suggesting the climate was warm and wet in the study area and an apparent marine sedimentary environment with relatively high sea level. Deciduous *Quercus* dominated the interval of 17–12 m, which indicated that the climate was relatively cool, corresponding to the end of Marine isotope stages3 (MIS3) to the Last Glacial Maximum accompanied by weathering and denudation. Above 12 m, the low pollen concentration with increased marine dinoflagellate cysts and foraminifera abundance suggested a marine sedimentary environment in the Taiwan Shoal. The high concentrations in *Pinus* corresponds to Holocene high sea level.

**Keywords:** Late Pleistocene; major and trace elements; pollen; principal component analysis; Taiwan Shoal



**Citation:** He, C.; Sha, L.; Zhao, D.; Dai, L.; Li, Z.; Tang, J.; Li, X.; Li, D. Sedimentary Environmental Evolution of the Western Taiwan Shoal Area since the Late Pleistocene. *J. Mar. Sci. Eng.* **2021**, *9*, 1150. <https://doi.org/10.3390/jmse9101150>

Academic Editor: Gemma Aiello

Received: 4 September 2021

Accepted: 14 October 2021

Published: 19 October 2021

**Publisher's Note:** MDPI stays neutral with regard to jurisdictional claims in published maps and institutional affiliations.



**Copyright:** © 2021 by the authors. Licensee MDPI, Basel, Switzerland. This article is an open access article distributed under the terms and conditions of the Creative Commons Attribution (CC BY) license (<https://creativecommons.org/licenses/by/4.0/>).

## 1. Introduction

The Taiwan Strait, a waterway between Mainland China and Taiwan, is a relatively shallow shelf sea (average 60 m in water depth) dominated by tidal currents [1]. It is considered an important channel for material and energy resource exchange (Figure 1). Interaction between the Kuroshio Current, South China Seawater and the Zhe-Min Coastal Current, and strong tidal currents prompts a large amount of sediment to accumulate at the narrows or shoals in the strait [2]. Wu [3] found that the distribution pattern of rare-earth elements in the Taiwan Shoal is similar to that of granite in Fujian and the East China Sea continental shelf. The foraminifera analysis of 16 cores in the western Taiwan Strait shows that the strata of the Taiwan Strait since the late Quaternary can be divided into five layers, and the Taiwan Strait was a neritic environment in the Last Glacial period [4]. Lan et al. [5,6] also reported that the coarse sand at ~20 ka BP in the Taiwan Shoal contained

exotic substances, and there was no “land bridge” in the Taiwan Strait since the Late Pleistocene. At the same time, the sea level of the Taiwan Strait had been rising since the Holocene, reaching the modern level at 4–3 ka BP. In addition, according to Yang et al. [7], the magnetic susceptibility of surface sediments declined from the nearshore area to the seaward in the western Taiwan Strait, and the magnetic susceptibility was controlled by the source of sediments and sedimentation. Dong et al. [8] discussed the history of the sea-level change and coastline migration in southwest Taiwan during the Holocene, and the results show that southwest Taiwan experienced marine transgression three times in the Holocene (~6.2 ka, ~3.1 ka, and ~1.8 ka). Wang et al. [9] analyzed the stratigraphic sequence and the paleoenvironmental development of the Taiwan Shoal based on records of the grain size and the Accelerator Mass Spectrometry (AMS)  $^{14}\text{C}$  dating results. However, all the above studies are based on one or two proxies with deficient chronological results. In order to clarify the sedimentary environmental evolution of the Taiwan Shoal since the Late Pleistocene, multiproxy research is considered indispensable.

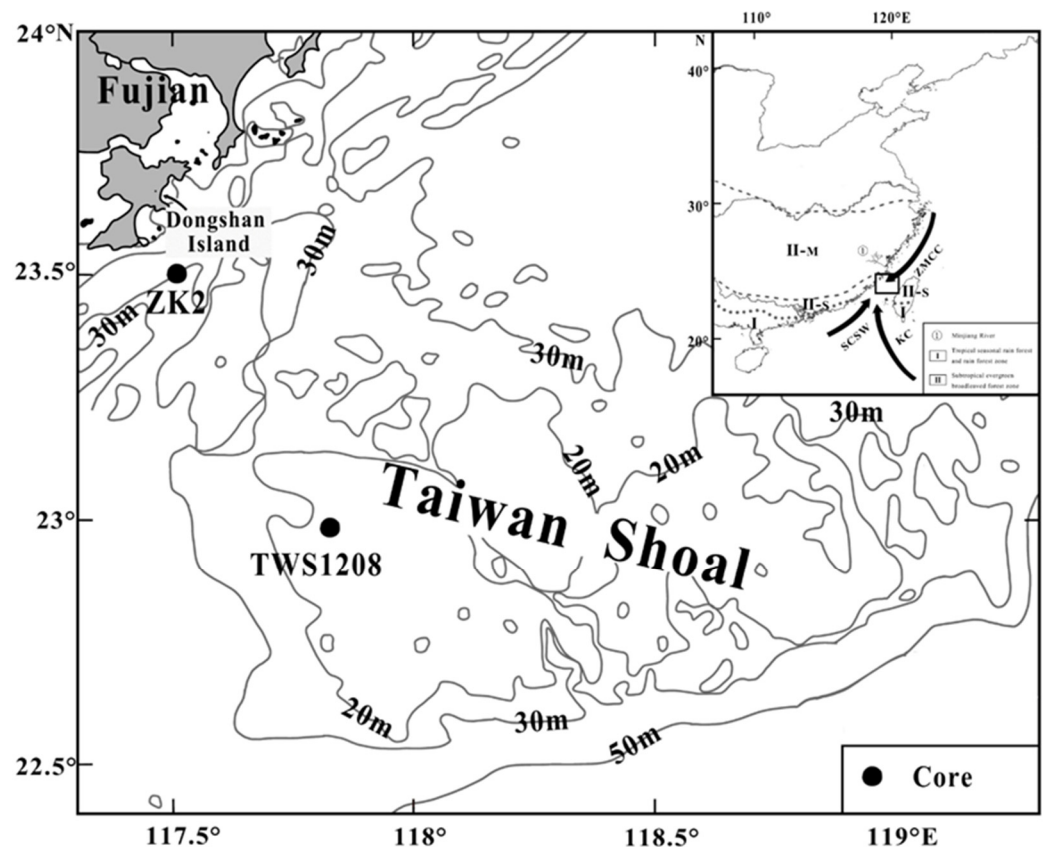


**Figure 1.** Map of the Taiwan Shoal and location of core ZK2 and TWS1208 [9]. ZMCC: Zhe-Min Coastal Current. SCSW: South China Sea water. KC: Kuroshio Current. Figure of vegetation zones in tropical and subtropical China is modified from Zheng [10] and Yue et al. [11].

Pollen in marine sediments comes from the surrounding land and coastal areas, so the surrounding vegetation is one of the basic factors that affect the distribution of pollen assemblages in marine sediments. In order to better clarify the process of the pollen transport from land to marine areas, many scholars have performed studies on pollen in marine areas to provide an adequate reference for the reconstruction of the paleoenvironment, such as in the Bohai Sea [12,13], the East China Sea [14], and the South China Sea [15–19]. However, in other areas, several studies have shown a good correlation between marine pollen signals and the nearby terrestrial vegetation [20–22]. However, in other areas, such as in the Gulf of Lions in southeastern France (the western Mediterranean Sea), the relationship between pollen signals and the inland vegetation

is not evident [23]. Jing et al. [24] studied the distribution patterns of pollen and spores in the northwestern Taiwan Strait based on 338 surface sediment samples. The results show that the pollen abundance is mainly affected by water depth and sediment grain size (texture). Lan et al. [6] studied the pollen assemblages of gravity cores in the western Taiwan Strait since the Late Pleistocene. However, the above studies have mainly analyzed the transportation and deposition processes in the Taiwan Strait, but a few of them have combined the paleontological records and geochemical proxies to infer the environmental and climatic change.

Previous works have mainly been focused on the modern sedimentary process of the Taiwan Strait, which was the junction of the East China Sea and the South China Sea. There are few research reports on the long-term stratigraphic structure and sedimentary environment evolution of the Taiwan Strait. Despite that the Taiwan Shoal in the southern Taiwan Strait is one of the world's famous submarine shoals, the changes in the paleoenvironment of the Taiwan Shoal have been scarcely studied because of discontinuous formation and lack of precise and accurate age-depth model. In this study, we obtained a sedimentary core ZK2 from the Taiwan Shoal area and reconstruct the paleoenvironmental evolution of the Taiwan Shoal by palynological and geochemical analysis. The aim of research was to provide a multi-proxy reconstruction of the evolution of the sedimentary environment in the Taiwan Shoal since the Late Pleistocene and provide scientific references for future studies.

## 2. Geographical Setting

The Taiwan Shoal in the southern Taiwan Strait represents one of the sedimentary subregions [1,25], and it is the shallowest part of the Taiwan Strait. Meanwhile, as one of the world's famous submarine shoals, the Taiwan Shoal is the junction of the East China Sea and the South China Sea. Furthermore, the Taiwan Shoal is adjacent to the Zhangpu coastal area of the southern Fujian in the west and extends to the Penghu Islands in the middle of the Taiwan Strait in the east. It measures about 250 km long from east to west, 135 km wide from north to south, and covers an area of about 13,000 km<sup>2</sup>. Moreover, the bottom of the Taiwan Shoal is mainly sandy coarse-grained sediments [26], and it is obviously different from the sedimentary layers of other sea areas in China. The Taiwan Shoal, with a water depth of only 10–25 m, is an uplifted area of the Taiwan Strait, and some geological records are missing due to the repeated transgressions and retreats [2].

The direction of the surface and bottom ocean currents shows apparent differences in the Taiwan Shoal due to the combined effect of the South China Seawater, the Kuroshio Current, and the Zhe-Min Coastal Current. The surface ocean current possesses the characteristics of the wind-driven current in summer and flows northeast, whereas it flows southward in winter under the control of the Zhe-Min Coastal Current. Meanwhile, the bottom ocean current flows northward throughout the year. In winter, it is affected by the extended South China Sea warm current and presents a different flow direction from the surface current [27]. The study area, with an intense tide action, experiences an irregular semi-diurnal tide, which is dominated by the M2 sub-tide, the average annual tidal level is 0.46 m, the average tidal range is 2.33 m, the average annual tidal current velocity is 0.46 m/s, and the maximum can be up to 0.8 m/s [28]. The Taiwan Shoal belongs to the southern tropical oceanic monsoon climate, with a mild and humid climate and plentiful rainfall. The annual average air temperature is estimated as 21.2 °C, and the average air temperatures of the hottest months (July–August) and the coldest months (January–February) are estimated as 27 °C and 13 °C, respectively. The annual average precipitation is estimated as 1071 mm, and the precipitation in spring and summer accounts for 61% of the total precipitation throughout the year. The prevailing wind is mostly in the northeasterly wind direction and it is strong throughout the year. The multi-year average of windy days is estimated as 122 days, with an annual average wind speed of 7.1 m/s, and typhoons and storm surge activities in the study area are frequent [2].

Vegetation in the southeastern monsoon region of China belongs to tropical and subtropical forests. The natural forest components from south to north in southern China

are mainly rainforests, seasonal rainforests, evergreen seasonal rainforests, and evergreen broad-leaved forests. The vegetation partition is shown in Figure 1 [10,11]. As a marine sedimentary area, the palynology of the Taiwan Shoal comes from I (tropical seasonal rain forest and rain forest), II-M (evergreen broadleaved forest), II-S (monsoon subtropical evergreen broadleaved forest) [10,11,29].

### 3. Materials and Methods

A 40 m long gravity core, core ZK2 (23°30′38.44″ N, 117°30′55.94″ E), was collected from the coast of the Dongshan Island, Fujian, in June 2015. The core is located in the northwest of the Taiwan Shoal, with a water depth of 37.5 m and a column length of 40 m. In this analysis, samples were collected at an interval of 2 m, and a total of 20 samples were collected.

All pollen samples were dried and weighed. Then, an exotic *Lycopodium*-spore tablet as a maker containing  $27,637 \pm 593$  grains was added to each sample in order to permit the estimation of the pollen concentration before preparation, followed by an alternative treatment with HF (40%) and HCl (10%). For sandy samples, they are first elutriated, and suspended solids are separated, precipitated, and then chemically treated. Subsequently, the residue of the sample is cleaned and placed in an ultrasonic oscillator. The remaining impurities are removed by using a 7  $\mu\text{m}$  mesh sieve, and finally, pollen grains are deposited. The pollen identification process was performed under a 400 $\times$  Leica optical microscope, and each sample counted to at least 200 grains. Fern spores, the freshwater phytoplanktonic remains and dinoflagellate cysts were also identified on the pollen slides.

ELAN 9000 ICP-MS (PE Company, Groton, CT, USA) was used for the micro-element determination. The operating steps were as follows: 0.0400 g of the sample was accurately weighed and placed in a Teflon cup, 1.5 mL of HF and 0.5 mL of HNO<sub>3</sub> were added, and the mixture was sealed and digested to at 150 °C for 12 h and then cooled. The Teflon cup was taken out, the product was weighed and diluted to 40 g (dilution factor was about 1000), and then applied to the micro-element determination by using ICP-MS. The sensitivity of the ICP-MS instrument was adjusted to 1 ng mL<sup>-1</sup> 115 In 30,000 cps. The testing results of GBW07315 (sediment), GBW07316 (sediment), and BHVO-2 (basalt) were found to be consistent with the recommended values. The relative errors of most element determination results were within 5–10%.

The trace element determination was performed by using the IRIS Intrepid II XSP ICP-OES (Thermo Electron, Waltham, MA, USA), and the steps were the same as those of the trace element determination. The testing results of Al<sub>2</sub>O<sub>3</sub>, CaO, MnO, TiO<sub>2</sub>, GBW07315 (sediment), GBW07316 (sediment), and BHVO-2 were identical to those of the recommended values. The relative errors of the testing results were smaller than 2%.

Five accelerator mass spectrometry (AMS) <sup>14</sup>C data were measured by using the core ZK2. The age-dating materials were benthic foraminifera and charcoal (surface). Samples were sent to Beta Analytic, Miami, FL, USA, for completing the test. All <sup>14</sup>C ages were corrected into the calendar years by using the OxCal 4.4 software (available online: <https://c14.arch.ox.ac.uk/oxcal/OxCal.html> (accessed on 15 October 2021)) with 95.4% probability (High Probability Density Range Method (HPD): MARINE 20) (Table 1). The global oceanic carbon reservoir deviation ( $\Delta R$ ) was  $113 \pm 37$  an according to the data on the northwest coast of Taiwan [30]. The <sup>14</sup>C age at layer 36.5 m was >43,500 a BP, out of the AMS<sup>14</sup>C dating range, so the age-dating result at layer 36.5 m was excluded.

In this study, Past, a free software [31], is used to conduct Principal component analysis (PCA) on the contents of major and trace elements in core ZK2, in order to determine the ecological environmental implication of the principal component axis and provide a quantitative/semi-quantitative study of environmental indicators.

**Table 1.** AMS  $^{14}\text{C}$  ages of core ZK2. IRMS: Isotope Ratio Mass Spectrometry.

Core	Depth (m)	Laboratory Code	Dated Materials	$^{14}\text{C}$ Age (a BP)	IRMS $\delta^{13}\text{C}$ (‰)	Calibrated Age (cal a BP)
ZK2	3.5	Beta-496141	Benthic foraminifera	$3780 \pm 30$	−0.6	3701–3388
ZK2	7.5	Beta-496142	Benthic foraminifera	$4540 \pm 30$	0.1	4599–4186
ZK2	17.5	Beta-496143	Benthic foraminifera	$35,790 \pm 280$	0.3	40,410–39,304
ZK2	20.5	Beta-491937	Benthic foraminifera	$35,910 \pm 280$	−0.5	40,494–39,383
ZK2	36.5	Beta-491938	Charcoal	>43,500	−25.4	>43,500

## 4. Results

### 4.1. Palynomorph Composition and Concentration

All samples from the core ZK2 (excluding samples ZK2-25, ZK2-27 and ZK2-29) were found to contain pollen, and 56 pollen taxa were identified (Figure A1). Fern spores, the freshwater phytoplanktonic remains (mainly *Concentricystes*), and dinoflagellate cysts (mainly *Spiniferites*) were also found in the core ZK2. Among them, *Concentricystes* is an algal zygospore of the probable zygnematacean affinity [32]. Fossils of *Concentricystes* are widely distributed in the Cenozoic of eastern China [33] and are commonly found in the soil and black silt in the lake or river sections. *Concentricystes* is thus indicative of freshwater lakes or swamps on flood plains.

Arboreal pollen dominates the pollen assemblages, in which tropical and subtropical broad-leaved pollen taxa are the most abundant (47.34% in average), followed by the *Pinus* pollen (14.54% in average). However, changes in the contents of *Pinus* do not provide any climate information because *Pinus* communities are very common [34]. The average content of the temperate broad-leaved pollen is 10.38%. In addition, there was a low content of coniferous components at high altitudes and tropical and subtropical coniferous components, with an average content of 0.33% and 2.31%, respectively. Tropical and subtropical broad-leaved pollen taxa are dominated by evergreen *Quercus* with an average percentage of 35.19%. The most abundant temperate broadleaved taxa are deciduous *Quercus*, *Alnus*, *Ulmus*, and *Carpinus*. As compared to arboreal pollen, the contents of the herb pollen were relatively low (24.12% on average). The most abundant terrigenous herb taxa are Poaceae, Cyperaceae, Chenopodiaceae, and *Artemisia*, whereas the aquatic herb (mainly *Typha*) appears occasionally.

High concentrations of pollen were mainly observed in depth ranges of 22.5–12.5 m and 38.4–32.4 m; especially they were higher between the depths of 12.5 and 22.5 m. In addition, marine dinoflagellate cysts and the freshwater phytoplanktonic remains were mainly observed above the depth of ~22.5 m.

Palynomorph assemblages recovered from the Taiwan Shoal can be divided into the following three general groups (Figure 2):

#### 4.1.1. Zone I: (40–30 m)

High pollen concentrations (9530 grains/g on average) between samples in this zone indicate a stable sedimentary environment in the Taiwan Shoal. In the pollen assemblage, evergreen *Quercus* was absolutely dominant, with an average content of 55.40%, and other tropical and subtropical broad-leaved forests were found sporadically. *Pinus* is the second dominant component, with an average content of 16.54%. However, high-altitude coniferous forest, tropical and subtropical coniferous forest, temperate components, herbs and fern spores were all found sporadically in this zone. In addition, no marine dinoflagellate cysts were found in this zone.

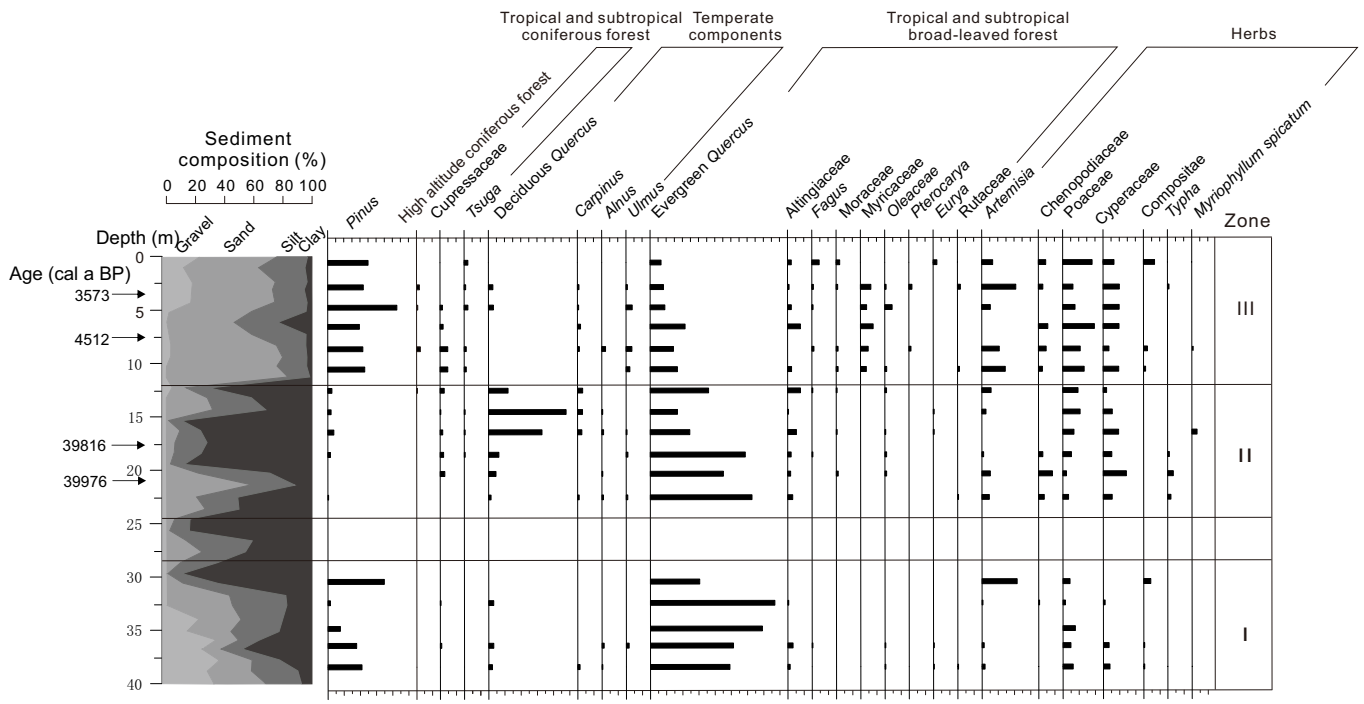


Figure 2. Pollen concentration diagram of core ZK2, and figure of sediment composition is modified from Zhao et al. [2].

#### 4.1.2. Zone II (24.5–12.5 m)

The pollen concentration was also relatively high but lower than that in zone I. Evergreen *Quercus* also dominated the pollen assemblage, with the average content as high as that in zone I, reaching 52.34%. Another tropical and subtropical broad-leaved tree taxon Altingiaceae was obviously increased in this zone. The content of temperate broad-leaved pollen increased remarkably as compared to that in zone I, and the main component was deciduous *Quercus*, with an average content of 17.57%. The content of *Pinus* shows an obvious decrease (1.75% on average). The content of terrestrial herbs shows a clear increase relative to that in zone I (19.05% on average), where the main components were Cyperaceae (7.06%) and Poaceae (6.36%). The aquatic herbs in this zone were more abundant than those in zone I. The contents of high-altitude conifers, tropical and subtropical conifers, and fern spores were also found occasionally. However, the concentration of the freshwater phytoplanktonic remains was high in this zone, and marine dinoflagellate cysts were found sporadically.

#### 4.1.3. Zone III (12.5–0 m)

The pollen concentrations in this zone were much lower than those in zones I and II. The content of the most abundant tropical and subtropical broad-leaved pollen taxa evergreen *Quercus* decreased remarkably, with an average content of 12.86%. However, the contents of the other tropical and subtropical broad-leaved pollen taxon increased as compared to those in zones I and II, especially the content of Myricaceae. The concentration of *Pinus* was much higher than that in zone II, with an average content of 25.66%. The content of temperate broad-leaved pollen was lower than those in zones I and II, with an average content of 4.45%. The contents of terrestrial herbs, mainly Poaceae (12.66%), Cyperaceae (8.32%), and *Artemisia* (9.76%), were higher than those in zones I and II, with an average content of 35.87%. The content of fern spores was 27.31%, which was also higher than those in zones I and II. The concentration of the freshwater phytoplanktonic remains was much lower than that in zone II, whereas the concentrations of marine dinoflagellate cysts were slightly lower than that in zone II.

#### 4.2. Major and Trace Element Contents

The vertical variations of major element contents in the core ZK2 are shown in Figure 3. The average content of oxides of major elements was found in the following order:  $\text{SiO}_2 > \text{Al}_2\text{O}_3 > \text{CaO} > \text{TiO}_2 > \text{MnO}$ . Among them,  $\text{SiO}_2$  was the most abundant composition, ranging from 61.04% to 89.11% (74.24% on average).  $\text{Al}_2\text{O}_3$  ranged between 2.55% and 16.77% (10.08% on average). The content of  $\text{CaO}$  was observed between 0.1% and 3.02% (0.9% on average). The variation range of  $\text{TiO}_2$  was between 0.09% and 0.96% (0.57% on average). The  $\text{MnO}$  content was between 0.02% and 0.19% (0.05% on average).

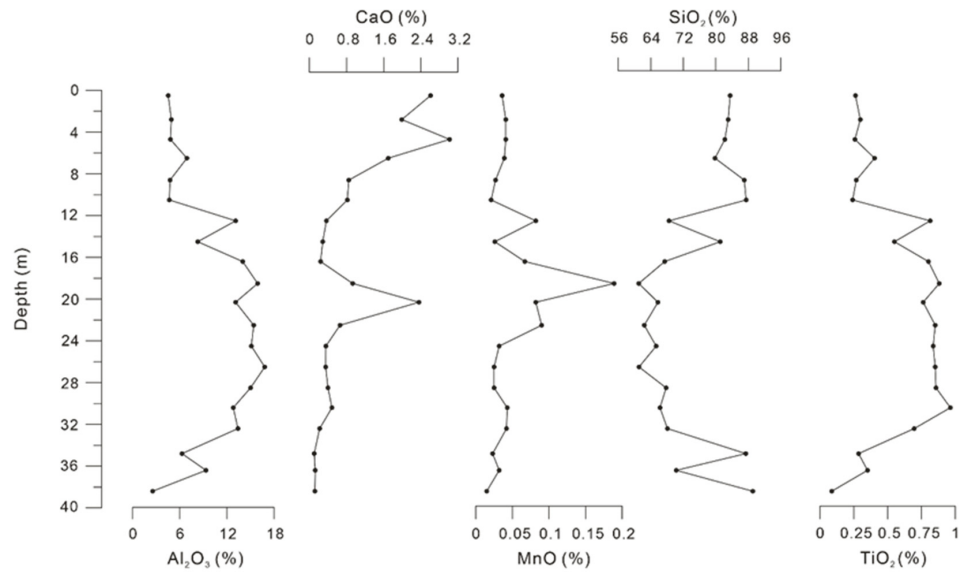


Figure 3. Changes in major element contents of core ZK2.

Figure 4 shows the variability of trace element contents in the core ZK2 since the Late Pleistocene. The contents of Ba were high, and most depths were above 200 mg/kg, with an average content of 342.9 mg/kg. The contents of Rb, Sr, Cu, Ni, and V were relatively low, with the average contents of 96.2, 85.8, 13.2, 23.1, and 62.8 mg/kg, respectively. The variation characteristics of trace elements were found generally consistent, indicating a gradually increasing trend at a depth of 40–20 m, followed by a reduction above the depth of ~20 m.

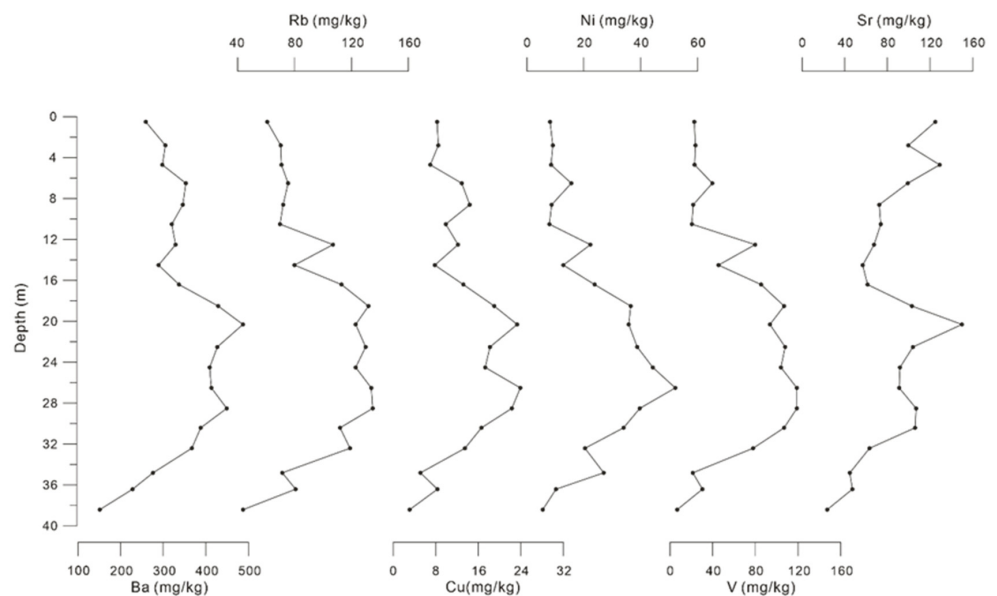


Figure 4. Changes in trace element contents of core ZK2.

### 4.3. Principal Component Analysis

Principal component analysis was carried out in order to clarify the environmental implications of major and trace elements in core ZK2, and the scores of each element on the PCA axes (axis 1 and axis 2) are shown in Figure 5. The principal component loading diagram (Figure 5) shows the relationship between different elements, where each vector axis represents each element, and the horizontal and vertical axes (axis 1 and 2) represent the most important principal components. The length of the vector axis is proportional to the content of the element it represents. The angle between each vector and the coordinate axis represents the correlation between elements and between elements and each principal component. When the included angle is  $90^\circ$ , it indicates that there is no obvious correlation between the two elements. Less than or greater than  $90^\circ$  indicates that the two elements are positively or negatively correlated, and the quantitative relationship between the elements and environmental variables is obtained by its projection on the principal component axis.

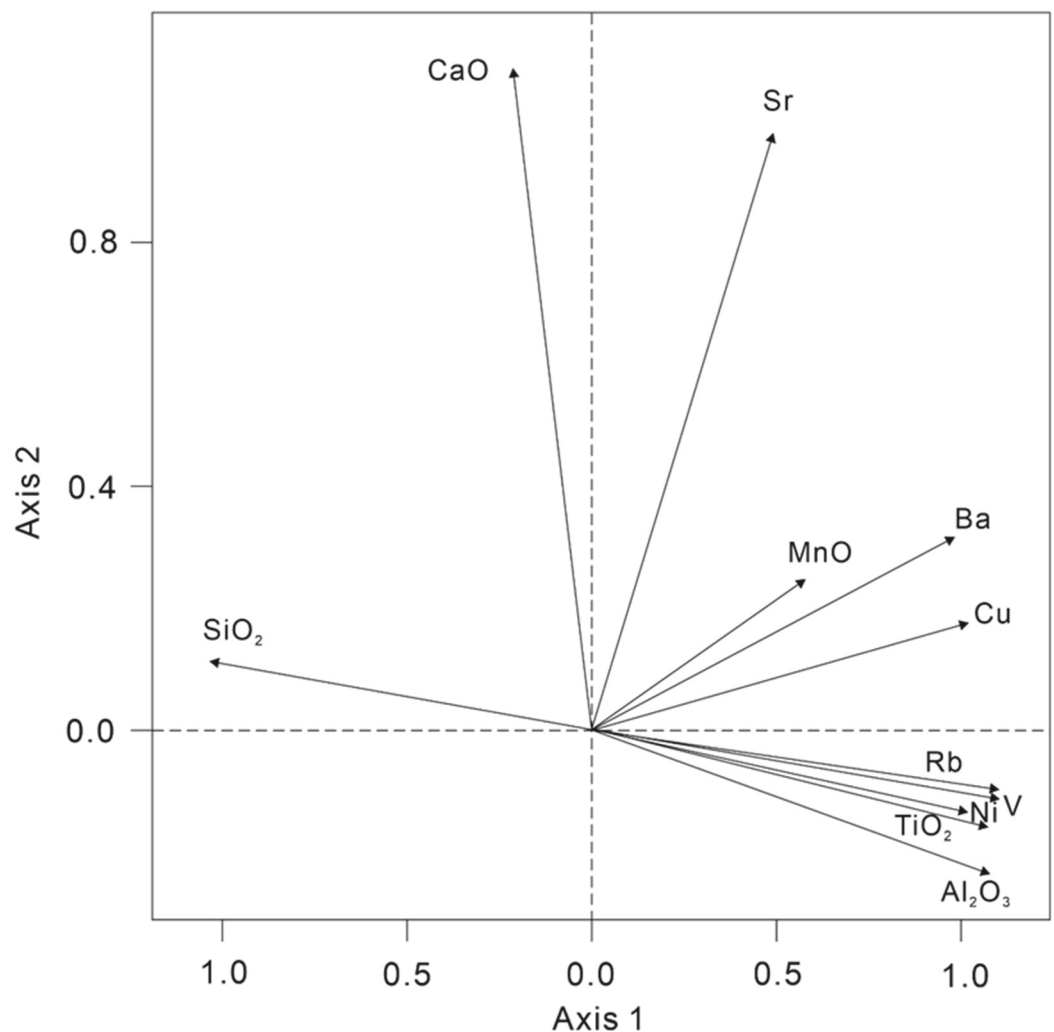


Figure 5. Principal component analysis (PCA) of major and trace elements scatter diagram.

The cumulative contribution rates of the first and second principal components to the total variance of all elements accounted for 87.36%, with 69.44% of axis 1 and 17.91% of axis 2, respectively. The contribution rates of other principal components are relatively low. This shows that the first and second principal components can explain most of the environment information contained in major and trace elements.

In the scatter diagram of axis 1 against axis 2, axis 1 is positively correlated with Al<sub>2</sub>O<sub>3</sub>, TiO<sub>2</sub>, MnO, Cu, Rb, Ni, V, and Ba, but negatively correlated to SiO<sub>2</sub> (Figure 5). Changes in



the contents of SiO<sub>2</sub> were negatively correlated with the other elements, and the content of SiO<sub>2</sub> was generally proportional to the sediments with large grain sizes, whereas other elements were proportional to the finer sediments [35]. MnO and Al<sub>2</sub>O<sub>3</sub> are elements with relatively stable geochemical properties under the supergene condition, and they are mainly found in terrigenous debris and clay minerals. TiO<sub>2</sub> is believed to be derived from terrestrial debris [36–39]. Generally, the alkali earth element Ba in marine sediments is often associated with autogenous effects, such as biological productivity [39–41], and Cu is considered an essential element for phytoplankton [42,43]. Therefore, axis 1 may be associated with the input of terrigenous materials or primary productivity and authigenic deposition. Axis 2 is positively correlated to CaO and Sr (Figure 5), which are closely related to the action of marine organisms [42,44]. CaO is considered an important constituent of biological carbonate, and Sr transforms into carbonate shells and bones after it is absorbed by organisms. Therefore, it was concluded that axis 2 could be represented by marine biogenic matters.

### 5. Discussion

The pollen record of the core ZK2 indicated that arboreal pollen dominated the Late Pleistocene, which was possibly carried by the Zhe-Min Coastal Current and the surrounding rivers near the study area [6,24]. The core ZK2 can be divided into the following five deposition units according to the comprehensive analysis of pollen and major and trace element results (Figure 6).

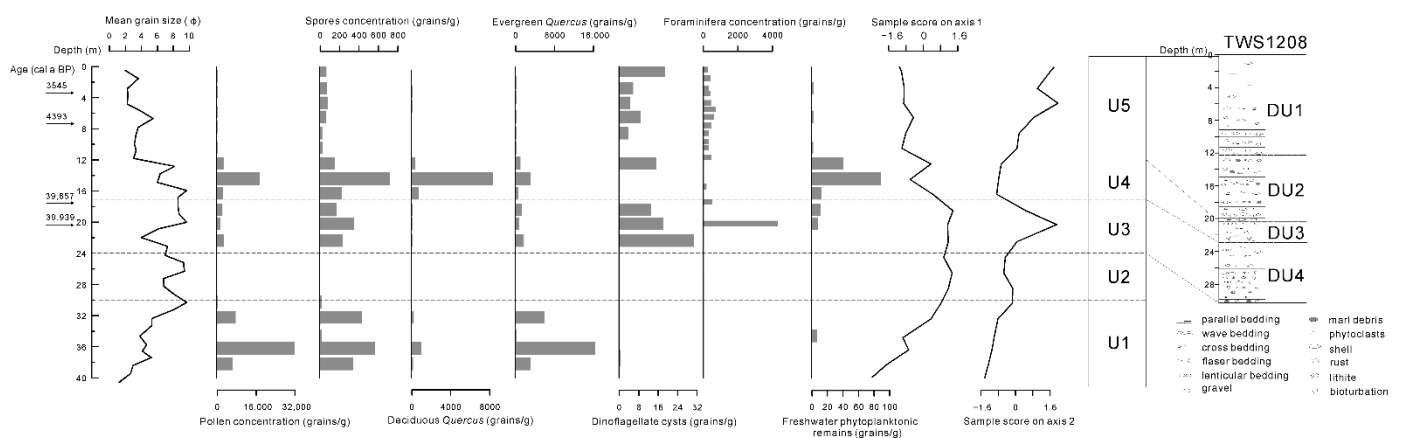


**Figure 6.** Mean grain size, major and trace elements and pollen and foraminifera concentrations of core ZK2 compared with the stratigraphic of core TWS1208 [9]. Figure of the mean grain size and TWS1208 is modified from Zhao et al. [2] and Wang et al. [9], respectively.

In phase U1 (40–30 m), pollen and spore concentrations were high, which indicates an almost unchanged terrestrial sedimentary environment. The high abundance of evergreen *Quercus* in this phase indicated that the surrounding area was covered by a tropical and subtropical broad-leaved forest (Figure 2). This is consistent with a pollen record in the Minjiang River estuary, where the pollen species of the Late Pleistocene strata are mainly *Pinus*, *Cupressaceae*, *Quercus* and *Polypodiaceae* [45]. Lan et al. [6] studied the pollen assemblages of gravity cores in the western Taiwan Strait since the Late Pleistocene, which reveals a *Quercus*, *Pinus*–*Polypodiaceae* assemblage during the MIS 3. The vegetation evolution study of Fuzhou Basin shows that the primary and mixed forests with deciduous and evergreen elements covered the mountainous areas with relatively warm and humid climate in MIS3 period, which is also consistent with the pollen record of this study [11]. In addition, no marine dinoflagellate cysts and foraminifera [2] were found in this phase (Figure 6), accompanied by a very low content of the representative marine sedimentary element CaO (Figure 3), which suggest no marine influence in the Taiwan Shoal. The low sample score on axis 2 also suggests a lack of the marine biogenic matter source. In this

phase, the high chemical index of illite indicated that chemical weathering was strong and the contents of unstable minerals epidote and hornblende also shows the near-source characteristics [2]. Therefore, we can conclude that the Taiwan Shoal might have been a terrigenous sedimentary environment in this phase, corresponding to the stratigraphic D layer of the late Quaternary in the western Taiwan Strait [46].

There was a disappearance of pollen and spores, as well as marine dinoflagellate cysts and foraminifera [2] in phase U2 (30–24 m). It has been reported that once pollen and spores are deposited into water, they behave similarly to small sediment particles of clay and fine silt [13]. This observation suggests that the sedimentation of pollen and spores in marine waters is controlled by mechanisms similar to those that control the sedimentation of clay and fine silt [20]. Strong boundary currents or coastal currents have a considerable impact on pollen sediment [47]. Phase U2 with coarse particle size (Figure 6) without pollen is deposited because of the strong hydrodynamic suspension and screening for sediments and pollen. A slight increase in sample score on axis 1, accompanied by a slight decrease in sample score on axis 2, suggested that the source of sediments in the Taiwan Shoal area fluctuated slightly during this period. Most intense chemical weathering results in a preponderance of aluminous clay minerals, and physical weathering leads to silicate enrichment [48,49]. Therefore, a slight increase in  $\text{Al}_2\text{O}_3$  and  $\text{TiO}_2$  as compared to a decrease in  $\text{SiO}_2$  in this phase would imply the enhanced chemical weathering under warm and humid weather [50]. In addition, according to Zou et al. [51] and Liang et al. [52], the elements Ni and V can be easily accumulated under a reducing environment and positively correlated to fine-grained sediments. The contents of CaO and Sr, as well as sample score on axis 2, showed little change in this phase (Figures 3, 4 and 6), which implies no marine influence in the Taiwan Shoal area.

The reappearance of pollen and spores, including evergreen *Quercus* in phase U3 (24–17 m) implied a warm and wet conditions, and the study area was covered by the tropical and subtropical broad-leaved forest, corresponding to the sedimentary unit DU4 (Coastal-intertidal deposits) of the core TWS1208 in the western Taiwan Shoal [9]. The pollen record of the Pingnan County, Fujian Province of southern China, also indicates that Fujian was covered by a mixed forest containing both subtropical evergreen and temperate deciduous broad-leaved trees prior to the Last Glacial Maximum [11], supporting the appearance of evergreen *Quercus* at this stage in the Taiwan Shoal area. Marine dinoflagellate cysts and foraminifera appeared with an abrupt increasing trend, suggesting an enhanced marine influence in the study area, corresponding to the stratigraphic C layer of the late Quaternary in western Taiwan Strait [46]. The contents of  $\text{Al}_2\text{O}_3$ , MnO,  $\text{TiO}_2$  and Rb were low, indicating a slight reduction in the input of terrigenous debris at that time (Figures 3 and 4). In contrast, the contents of CaO and Sr reached their peak values, which indicates an enhanced marine influence in the 24–18 m interval. The sample score on axis 1 was stable, whereas the sample score on axis 2 increased abruptly and reached the maximum in this phase, which suggests a remarkable increase in the marine influence in the Taiwan Shoal. Furthermore, a pollen record along the Fujian seashore shows a subtropical evergreen broad-leaved forest during that period, which represents the warm and humid climate [46]. Since the age control of 20.5 m was 40 cal ka BP, the 24–18 m interval possibly corresponds to the MIS 3 [53], and the Taiwan Shoal appeared in a subtidal environment during that period. The mean grain size fluctuated greatly during the 24–18 m interval [2] (Figure 6), which suggests an unstable depositional environment in the Taiwan Shoal. Previous studies from the coastal areas of Fujian also recorded the last transgression of the Late Pleistocene at 44–22 cal ka BP [53–55]. Coincidentally, the Chao-shan Plain has also recorded sea level rise, indicated by marine microfossils such as diatoms, foraminifera, and mangroves representing the coastal environment [56]. Therefore, the Taiwan Shoal was a coastal environment in phase U3 and herbs deposited in this area were carried by nearby rivers [57].

In phase U4 (17–12 m), deciduous *Quercus* concentrations increased gradually, reaching the maximum at a depth of 15 m. This indicated a relatively cold and dry condition

in the Taiwan Shoal, which would have allowed the temperate deciduous taxa to expand. The pollen record in Fujian also suggests that a deciduous forest prevailed during this period [11], and there was a *Pinus*–*Polygonaceae*–*Pteridium* assemblage in the western Taiwan Strait during the MIS 2 [6]. There were no marine dinoflagellate cysts and foraminifera found in this phase [2], whereas the freshwater phytoplanktonic remains were relatively abundant, which implies that the Taiwan Shoal was a fresh water environment between 15 and 12 m, possibly corresponding to the terrestrial deposit in the MIS 2 [2] and the sedimentary unit DU3 (Valley filling deposit) of the core TWS1208 in the western Taiwan Shoal [9]. In addition, an increase in the content of SiO<sub>2</sub> in this phase (Figure 3) indicated a high physical weathering degree, whereas a low content of Al<sub>2</sub>O<sub>3</sub> indicated a weak chemical weathering degree (Figure 3). According to the analysis of clay minerals, the increase in contents of unstable minerals epidote and hornblende indicates that the distance of sediment transport was closer, suggesting a continental sedimentary environment at the end of MIS3 or the beginning of the LGM [2]. Furthermore, low contents of CaO and Sr (Figures 3 and 4), as well as obviously declined sample score on axis 2, suggest little marine influence in this phase. Although the age of the top of phase U4 is unable to be examined accurately, clay minerals records show that the top of phase U4 was characterized by relative higher contents of illite and lower content of kaolinite than that in the modern, suggesting a close distance of sediment transport and strong physical weathering [2]. The reflected seismic data of the nearby core TWS1208 show the unit DU3 was exposed and subjected to intense weathering erosion [9]. In addition, the LGM strata with strong weathering and denudation also occurred in Chao-shan Plain, southwest of the study area [56]. Consequently, a long time interval between the two <sup>14</sup>C dating points on the upper part of the core may be contributed to the strong weathering and denudation between U4 and U5 (Figure 2).

Pollen and spore concentrations declined dramatically in phase U5 until they were absent in the upper part of the core, whereas the pollen record shows a mixed South subtropical evergreen coniferous-broad-leaved forest along the Fujian seashore [46]. The grain size of ZK2 analysis shows that this phase mainly consists of medium-coarse sands and gravelly medium-coarse sands [2] (Figure 2). Previous studies showed that the sediment environment with larger grain size was not conducive to the deposition of palynology; pollen is scarce in coarse clastics and abundant in marine sediments composed primarily of fine silt and clay-size particles [20]. In addition, ZMCC as a strong boundary current of the area is also one of the main reasons for the decrease of palynology concentration because the strong hydrodynamic environment is not conducive to the deposition of palynology [13]. However, the content of *Pinus* was 19.6–42.7% in phase U5, which is much higher than that in U4 (2–3.7%) (Figure 2). Previous studies have shown that *Pinus* can be used as an indicator of sea level changes during the glacial-interglacial period, and the proportion of *Pinus* will increase as the increase of the distance from the shore because of its airbags, which facilitate the propagation of wind [18]. Therefore, the increase in *Pinus* at this phase is probably related to the sea level rise. The offshore distance of the study area increased, and the amount of terrestrial pollen brought by land runoff decreased greatly, while the proportion of airborne pollen (*Pinus*) increased.

Relatively high abundance of marine dinoflagellate cysts, foraminifera [2], as well as the contents of CaO and Sr (Figures 3 and 4) all exhibited an increasing trend in the 10.5–0 m interval, which suggests an increased marine influence on the study area. According to the dating control points, phase U5 corresponded to the Holocene. Increased sample score on axis 2 also indicates the enhanced marine influence or sea level rise (Figure 6). All the relative sea level reconstructions from Longhai Plain, Fuzhou Basin and Singapore show sea level rise at about 9 cal ka BP, with a minimum sea-level rise of 14.5 m between 9 and 7.3 cal ka BP in the Fuzhou Basin and about 17 m rise in sea level from 9.5 to 7 cal ka BP in Singapore [58–61], supporting the relatively high sea level in the Taiwan Shoal inferred by pollen and elements data in this study. Therefore, we deduced that the study area was below the sea level during phase U5, corresponding to the Holocene high sea-level stage.

This phase also corresponded to the sedimentary unit DU2 (transgressive sand body) and DU1 (modern tidal current sand body) of the core TWS1208 in the western Taiwan Shoal, which may be affected by strong tidal currents during the Holocene [9].

## 6. Conclusions

(1) The pollen record of the core ZK2 shows that arboreal pollen dominated since the Late Pleistocene, among them tropical and subtropical broadleaved pollen were the dominant taxa, accompanied with relatively low abundance of temperate broadleaved pollen. This implies that the Taiwan Shoal area has always had a subtropical climate.

(2) The principal component analysis (PCA) of the major and trace elements in the core ZK2 shows that changes in sample score on axis 1 are possibly associated with the input of terrigenous debris carried by the southward Zhe-Min Coastal Current and sample score on axis 2 could be indicated by marine biogenic matters in the Taiwan Shoal area.

(3) Five evolution phases of the sedimentary environment in the Taiwan Shoal area are divided on the basis of the analysis of pollen and major and trace element results with the combination of the AMS  $^{14}\text{C}$  dating results. Phase U1 (40–30 m) possibly corresponded to a terrestrial sedimentary environment. Phase U2 (30–24 m) was a transition between terrestrial and marine sedimentary environments, and coarser grain size and strong hydrodynamics sedimentary environment are not conducive to pollen preservation. Phase U3 (24–17 m) was a transgression period with a coastal-intertidal deposits sedimentary environment. Phase U4 (17–12 m) was a terrestrial and marine alternative phase and the land was exposed in the Last Glacial Maximum, with large sea-level fluctuations. Phase U5 (12–0 m) appeared under a marine sedimentary environment, with the sea level rising to the modern level.

**Author Contributions:** Conceptualization, C.H. and L.S.; methodology, C.H., L.D. and Z.L.; software, C.H.; validation, C.H. and D.L.; formal analysis, C.H. and L.S.; investigation, D.Z.; resources, L.S., L.D. and D.Z.; data curation, L.S., L.D., D.L. and D.Z.; writing—original draft preparation, C.H., L.S., Z.L. and D.L.; writing—review and editing, C.H., L.S., Z.L. and D.L.; visualization, J.T. and X.L.; supervision, L.S., D.Z. and D.L.; project administration, L.S., D.Z. and D.L.; funding acquisition, D.L. All authors have read and agreed to the published version of the manuscript.

**Funding:** This work was supported by the National Natural Science Foundation of China [Grant No. 41776193, 41876215], Science and Technology Planning Project of Fujian Province [Grant No. 2016R1006-2], Ningbo Natural Science Foundation of China [Grant No. 2018A610282] and the K.C. Wong Magna Fund in Ningbo University.

**Institutional Review Board Statement:** Not applicable.

**Informed Consent Statement:** Not applicable.

**Data Availability Statement:** The data presented in this study are available on request from the corresponding author. The data are not publicly available due to privacy.

**Acknowledgments:** The authors are thankful to Assistant Editor Marijana Ilic for her help. The comments and feedback from two anonymous reviewers significantly improved the manuscript.

**Conflicts of Interest:** The authors declare no conflict of interest.

Appendix A

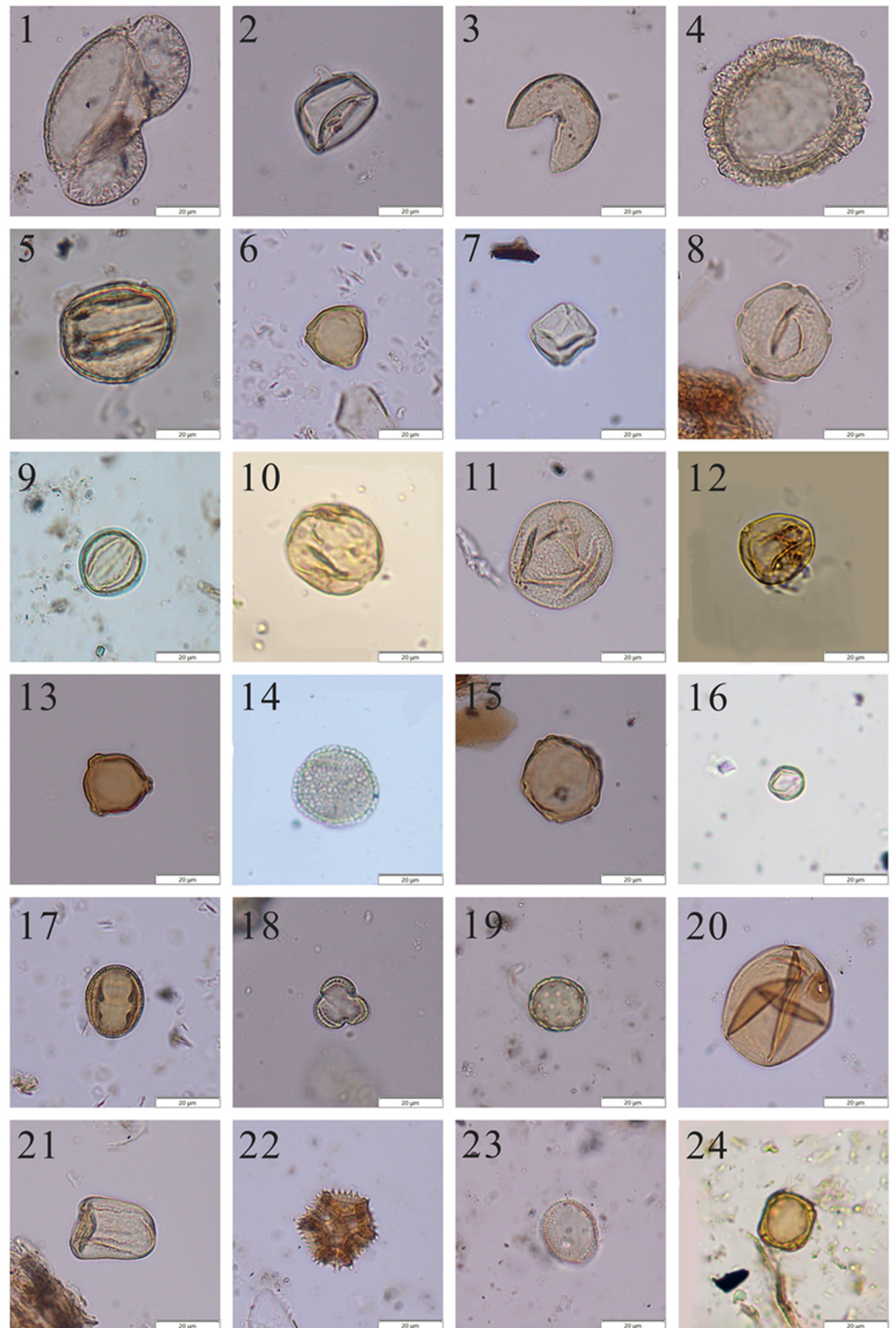


**Figure A1.** 1: Pinus; 2: Taxodiaceae; 3: Cupressaceae; 4: Tsuga; 5: Deciduous Quercus; 6: Myricaceae; 7: Alnus; 8: Ulmus; 9: Evergreen Quercus; 10: Altingiaceae; 11: Fagus; 12: Moraceae; 13: Carpinus; 14: Oleaceae; 15: Pterocarya; 16: Eurya; 17: Rutaceae; 18: Artemisia; 19: Chenopodiaceae; 20: Poaceae; 21: Cyperaceae; 22: Compositae; 23: Typha; 24: Myriophyllum spicatum.

## References

1. Liao, H.; Yu, H.; Su, C. Morphology and Sedimentation of Sand Bodies in the Tidal Shelf Sea of Eastern Taiwan Strait. *Mar. Geol.* **2008**, *248*, 161–178. [[CrossRef](#)]
2. Zhao, D.B.; Sun, R.T.; Jiang, H.Y. Sedimentary Characteristics and Paleoenvironmental Evolution of the Northwestern Taiwan Shoal Since the Late Pleistocene. *Mar. Geol. Quat. Geol.* **2020**, *40*, 1–12.
3. Wu, Q.M. Geochemistry of Rare Earth Elements in Seabed Sediments of Taiwan Shoal in My Country. *Geochemistry* **1983**, *3*, 303–313.
4. Chen, C.H.; Lan, D.Z.; Yu, Y.F.; Zhang, W.L. Late Quaternary Stratigraphy in the Western Taiwan Strait. *Quat. Sci.* **1990**, *10*, 301–307.
5. Lan, D.Z.; Zhang, W.L.; Chen, C.H.; Xie, Z.T. Preliminary Study on Age and Origin of Medium-Coarse Sands in Taiwan Shoal. *Taiwan Strait* **1991**, *10*, 54–59.
6. Lan, D.Z.; Zhang, W.L.; Chen, C.H.; Yu, Y.F. Transgression and Sea Level Change in the Western Taiwan Strait Since the Late Pleistocene. *Acta Oceanol. Sin.* **1993**, *15*, 77–84.
7. Yang, L.J. Distribution Characteristics of Magnetic Susceptibility of Surface Sediments in the Western Taiwan Strait. *Acta Sedimentol. Sin.* **2009**, *27*, 697–703.
8. Dong, D.H.; Deng, G.X.; Liu, M.Z. The Evolution of Paleoenvironment in Southwestern Taiwan Since the Holocene. *J. Subtrop. Resour. Environ.* **2012**, *7*, 1–9.
9. Wang, L.B.; Li, J.; Chen, Z.X.; Zhao, J.T.; Bai, F.L.; Hu, B.Q.; Dou, Y.G.; Zai, B. Late Pleistocene and Holocene Stratigraphy and Paleo-Environmental Evolution in the Western Taiwan Shoal. *Acta Sedimentol. Sin.* **2014**, *32*, 1089–1099.
10. Zheng, Z. Late Quaternary Vegetational and Climatic Changes in the Tropical and Subtropical Areas of China. *Acta Micropalaeontologica Sin.* **2000**, *17*, 125–146.
11. Yue, Y.F.; Zheng, Z.; Huang, K.Y.; Chevalier, M.; Chase, B.M.; Carré, M.; Ledru, M.-P.; Cheddadi, R. A Continuous Record of Vegetation and Climate Change over the Past 50,000 Years in the Fujian Province of Eastern Subtropical China. *Palaeogeogr. Palaeoclimatol. Palaeoecol.* **2012**, *365*, 115–123. [[CrossRef](#)]
12. Yang, S.X.; Li, J.; Liu, K.B.; Li, R.H.; Wen, Z.H.; Ye, S.Y.; Yi, S.; Chen, X.H. Pollen-Spore Distribution in the Surface Sediments of the Western Bohai Sea, China. *Quat. Int.* **2016**, *392*, 213–223. [[CrossRef](#)]
13. Yang, S.X.; Song, B.; Ye, S.Y.; Laws, E.A.; He, L.; Li, J.; Chen, J.X.; Zhao, G.M.; Zhao, J.T.; Mei, X.; et al. Large-Scale Pollen Distribution in Marine Surface Sediments from the Bohai Sea, China: Insights into Pollen Provenance, Transport, Deposition, and Coastal-Shelf Paleoenvironment. *Prog. Oceanogr.* **2019**, *178*, 102183. [[CrossRef](#)]
14. Wang, K.F.; Sun, Y.H.; Zhang, Y.L.; Jiang, H.; Zhang, Y.C. *The Spore-Pollen and Algal Assemblage in the East China Sea Sediments*; China Ocean Press: Beijing, China, 1987; pp. 10–80.
15. Luo, C.X.; Chen, M.H.; Xiang, R.; Liu, J.G.; Zhang, L.L.; Lu, J.; Yang, M.X. Characteristics of Modern Pollen Distribution in Surface Sediment Samples for the Northern South China Sea from Three Transects. *Quat. Int.* **2013**, *286*, 148–158. [[CrossRef](#)]
16. Luo, C.X.; Chen, M.H.; Xiang, R.; Liu, J.G.; Zhang, L.L.; Lu, J. Comparison of Modern Pollen Distribution between the Northern and Southern Parts of the South China Sea. *Int. J. Biometeorol.* **2015**, *59*, 397–415. [[CrossRef](#)] [[PubMed](#)]
17. Luo, C.X.; Lin, G.; Chen, M.H.; Xiang, R.; Zhang, L.L.; Liu, J.G.; Pan, A.D.; Yang, S.X.; Yang, M.X. Characteristics of Pollen in Surface Sediments from the Southern South China Sea and its Paleoclimatic Significance. *Palaeogeogr. Palaeoclimatol. Palaeoecol.* **2016**, *461*, 12–28. [[CrossRef](#)]
18. Sun, X.J.; Luo, Y.L.; Huang, F.; Tian, J.; Wang, P.X. Deep-Sea Pollen from the South China Sea: Pleistocene Indicators of East Asian Monsoon. *Mar. Geol.* **2003**, *201*, 97–118. [[CrossRef](#)]
19. Sun, X.J.; Li, X. Different Dynamics and Routes of Modern Pollen Transport in the Northern and Southern Parts of the South China Sea. *Sci. China Ser. D* **1998**, *41*, 494–498. [[CrossRef](#)]
20. Heusser, L.E. Pollen Distribution in Marine Sediments on the Continental Margin off Northern California. *Mar. Geol.* **1988**, *80*, 131–147. [[CrossRef](#)]
21. Sun, X.J.; Li, X. A Pollen Record of the last 37 ka in Deep Sea Core 17940 from the Northern Slope of the South China Sea. *Mar. Geol.* **1999**, *156*, 227–244. [[CrossRef](#)]
22. Van der Kaars, S. Pollen Distribution in Marine Sediments from the South-Eastern Indonesian Waters. *Palaeogeogr. Palaeoclimatol. Palaeoecol.* **2001**, *171*, 341–361. [[CrossRef](#)]
23. Beaudouin, C.; Suc, J.P.; Escarguel, G.; Arnaud, M.; Charmasson, S. The Significance of Pollen Signal in Present-Day Marine Terrigenous Sediments: The Example of the Gulf of Lions (Western Mediterranean Sea). *Geobios* **2007**, *40*, 159–172. [[CrossRef](#)]
24. Jing, X.; Chen, F.; Li, S.; Gui, Z.; Zhong, H. Distribution Pattern of Spore-Pollen in Surface Sediments of Northwestern Taiwan Strait and Its Geological Significance. *Mar. Geol. Quat. Geol.* **2014**, *34*, 81–88.
25. Liu, Z.X.; Xia, D.X.; Berne, S.; Wang, K.Y.; Marsset, T.; Tang, Y.X.; Bourillet, J.F. Tidal Deposition Systems of China's Continental Shelf, with Special Reference to the Eastern Bohai Sea. *Mar. Geol.* **1998**, *145*, 225–253.
26. Hu, Y.; Chen, J.; Xu, J.; Wang, L.; Li, H.; Liu, H. Sand Wave Deposition in the Taiwan Shoal of China. *Acta Oceanol. Sin.* **2013**, *32*, 26–34. [[CrossRef](#)]
27. Shi, Q.; Zhang, J.Y.; Cai, A.Z. Taiwan Shoal-Huge Sand Resource Pool. *J. Nat. Resour.* **2009**, *24*, 507–513.
28. Wang, Y.H.; Jan, S.; Wang, D.P. Transports and Tidal Current Estimates in the Taiwan Strait from Shipboard ADCP Observations (1999–2001). *Estuar. Coast. Shelf Sci.* **2003**, *57*, 193–199. [[CrossRef](#)]

29. Takahara, H.Y.; Igarashi, R.; Hayashi, F.; Kumon, P.M.; Liew, M.; Yamamoto, S.; Kawai, T.; Tadamichi, O.; Tomohisa, I. Millennial-Scale Variability in Vegetation Records from the East Asian Islands: Taiwan, Japan and Sakhalin. *Quat. Sci. Rev.* **2010**, *29*, 2900–2917. [[CrossRef](#)]
30. Yoneda, M.; Uno, H.; Shibata, Y.; Suzuki, R.; Kumamoto, Y.; Yoshida, K.; Sasaki, T.; Suzuki, A.; Kawahata, H. Radiocarbon Marine Reservoir Ages in the Western Pacific Estimated by Pre-Bomb Molluscan Shells. *Nucl. Instrum. Methods Phys. Res. Sect. B Beam Interact. Mater. At.* **2007**, *259*, 432–437. [[CrossRef](#)]
31. Hammer, Ø.; Harper, D.A.T.; Ryan, P.D. PAST: Paleontological statistics software package for education and data analysis. *Palaeontologia electronica.* **2001**, *4*, 9.
32. Qin, J.G.; Wu, G.X.; Zheng, H.B.; Zhou, Q. The Palynology of the First Hard Clay Layer (Late Pleistocene) from the Yangtze Delta, China. *Rev. Palaeobot. Palynol.* **2008**, *149*, 63–72. [[CrossRef](#)]
33. Wang, K.F.; Han, X.B. Study on the Cenozoic Fossil Concentricystes of East China. *Acta Palaeontol. Sin.* **1983**, *22*, 468–472.
34. Dai, L.; Weng, C.Y.; Lu, J.; Mao, L.M. Pollen Quantitative Distribution in Marine and Fluvial Surface Sediments from the Northern South China Sea: New Insights into Pollen Transportation and Deposition Mechanisms. *Quat. Int.* **2014**, *325*, 136–149. [[CrossRef](#)]
35. Zhao, Y.Y.; Che, C.H.; Yang, H.L.; Jia, F.M. Geochemistry of Fe, Mn, Ti, and P in the Taiwan Bank, China. *Acta Geol. Sin.* **1981**, *18*, 118–126.
36. Bhatt, J.J. Ti/Al Ratio as Chemical Index of Paleoenvironment-A Note. *Chem. Geol.* **1974**, *13*, 75–78. [[CrossRef](#)]
37. Schmitz, B. The TiO<sub>2</sub>/Al<sub>2</sub>O<sub>3</sub> Ratio in the Cenozoic Bengal A byssal Fan Sediments and Its Use as a Paleostream Energy Indicator. *Mar. Geol.* **1987**, *78*, 195–206. [[CrossRef](#)]
38. Wei, G.J.; Liu, Y.; Li, X.H.; Shao, L.; Fang, D.Y. Major and Trace Element Variations of the Sediments at ODP Site 1144, South China Sea, during the Last 230 ka and Their Paleoclimate Implications. *Palaeogeography Palaeoclimatol. Palaeoecol.* **2004**, *212*, 331–342. [[CrossRef](#)]
39. Yang, S.Y.; Lim, D.I.; Jung, H.S.; Oh, B.C. Geochemical Composition and Provenance Discrimination of Coastal Sediments around Cheju Island in the Southeastern Yellow Sea. *Mar. Geol.* **2004**, *26*, 41–53. [[CrossRef](#)]
40. Dymond, J.; Suess, E.; Lyle, M. Barium in Deep-Sea Sediment: A Geochemical Proxy for Paleoproductivity. *Paleoceanography* **1992**, *7*, 163–181. [[CrossRef](#)]
41. Dean, W.E.; Gardner, J.V.; Piper, D.Z. Inorganic Geochemical Indicators of Glacial-Interglacial Changes in Productivity and Anoxia on the California Continental Margin. *Geochim. Cosmochim. Acta* **1997**, *61*, 4507–4518. [[CrossRef](#)]
42. Sun, X.Q.; Liu, S.F.; Li, J.R.; Zhang, H.; Zhu, A.M.; Cao, P.; Chen, M.T.; Zhao, G.T.; Khokiattiwong, S.; Kornkanitnan, N.; et al. Major and Trace Element Compositions of Surface Sediments from the Lower Bengal Fan: Implications for Provenance Discrimination and Sedimentary Environment. *J. Asian Earth Sci.* **2019**, *184*, 104000. [[CrossRef](#)]
43. Li, H.J.; Hermann, J. The Effect of Fluorine and Chlorine on Trace Element Partitioning between Apatite and Sediment Melt at Subduction Zone Conditions. *Chem. Geol.* **2017**, *473*, 55–73. [[CrossRef](#)]
44. Guo, Z.G.; Yang, Z.S.; Qu, Y.H.; Fan, D.J. Study on Comparison Sedimentary Geochemistry of Mud Area on East China Sea Continental Shelf. *Acta Sedimentol. Sin.* **2000**, *18*, 284–289.
45. Yang, J.W.; Hua, L.; Wu, L.C. Sporopollen, Foram and Diatom Assemblages of Quaternary Strata in the Minjiang River Estuary and Its Paleo-Geographical Significance. *Mar. Geol. Quat. Geol.* **1991**, *11*, 75–83.
46. Wang, K.F.; Lu, J.J.; Zheng, Y.L. Late Quaternary Pollen-Diatom Assemblages along Fujian Seashore and Their Paleoenvironmental Implications. *Acta Micropalaeontologica Sin.* **1995**, *12*, 388–397.
47. Heusser, L.E.; Balsam, W.L. Pollen Sedimentation in the Northwest Atlantic: Effects of the Western Boundary Undercurrent. *Mar. Geol.* **1985**, *69*, 149–153. [[CrossRef](#)]
48. Nesbitt, H.W.; Markovics, G.; Price, R.C. Chemical Processes Affecting Alkalis and Alkaline Earths during Continental Weathering. *Geochim. Cosmochim. Acta* **1980**, *44*, 1659–1666. [[CrossRef](#)]
49. Nesbitt, H.W.; Young, G.M. Petrogenesis of Sediments in the Absence of Chemical Weathering: Effects of Abrasion and Sorting on Bulk Composition and Mineralogy. *Sedimentology* **1996**, *43*, 341–358. [[CrossRef](#)]
50. Tao, J.; Chen, M.T.; Xu, S.Y. A Holocene Environmental Record from the Southern Yangtze River Delta, Eastern China. *Palaeogeogr. Palaeoclimatol. Palaeoecol.* **2006**, *230*, 204–229. [[CrossRef](#)]
51. Zou, J.J.; Shi, X.F.; Li, S.L. Distribution of Minor Elements in Near Surface Sediments in north Yellow Sea and the Early Diagenesis. *Mar. Geol. Quat. Geol.* **2007**, *27*, 43–51.
52. Liang, W.J.; Xiao, C.T.; Xiao, K.; Lin, W. The Relationship of Late Jurassic Paleoenvironment and Paleoclimate with Geochemical Elements in Amdo Country of Northern Tibet. *Geol. China* **2015**, *42*, 1079–1091.
53. Lan, D.Z.; Yu, Y.F.; Chen, C.H.; Xie, Z.T. Preliminary Study on the Late Pleistocene Transgression and Holocene Sea-Level Fluctuation in Fuzhou Basin. *Mar. Geol. Quat. Geol.* **1986**, *6*, 103–110.
54. Yang, J.M. The Last Marine Transgression and Sea Level Changes along the Fujian Coast during Late Pleistocene. *Mar. Sci.* **1988**, *5*, 5–9.
55. Zeng, C.S. A Discussion on Problems of Marine Transgression along the Fujian coast during The Late Pleistocene. *Trop. Oceanol.* **1993**, *12*, 39–45.
56. Zheng, Z.; Li, Q. Vegetation, Climate, and Sea Level in the Past 55,000 Years, Hanjiang Delta, Southeastern China. *Quat. Res.* **2000**, *53*, 330–340. [[CrossRef](#)]

57. Zheng, Z.; Yang, S.X.; Deng, Y.; Huang, K.Y.; Wei, J.H.; Berne, S.; Suc, J.-P. Pollen Record of the Past 60 ka BP in the Middle Okinawa Trough: Terrestrial Provenance and Reconstruction of the Paleoenvironment. *Palaeogeogr. Palaeoclimatol. Palaeoecol.* **2011**, *307*, 285–300. [[CrossRef](#)]
58. Bird, M.I.; Fifield, L.K.; Teh, T.S.; Chang, C.H.; Shirlaw, N.; Lambeck, K. An Inflection in the Rate of Early Mid-Holocene Eustatic Sea-Level Rise: A New Sea-Level Curve from Singapore. *Estuar. Coast. Shelf Sci.* **2007**, *71*, 523–536. [[CrossRef](#)]
59. Rolett, B.V.; Zheng, Z.; Yue, Y.F. Holocene Sea-Level Change and the Emergence of Neolithic Seafaring in the Fuzhou Basin (Fujian, China). *Quat. Sci. Rev.* **2011**, *30*, 788–797. [[CrossRef](#)]
60. Ge, W.Y.; Li, C.H.; Xing, H.X.; Li, L.; Li, Y.X.; Rittenour, T.; Hu, Z.J. Examining the Chronology of Transgressions Since the Late Pleistocene in the Fujian Coast, Southeastern China. *Quat. Int.* **2019**, *527*, 34–43. [[CrossRef](#)]
61. Zong, Y.Q. Mid-Holocene Sea-Level Highstand along the Southeast Coast of China. *Quat. Int.* **2004**, *117*, 55–67. [[CrossRef](#)]